Copy
RM E53D13

NACA RM E53D13

6810

NACA

RESEARCH MEMORANDUM

INVESTIGATION OF 16-INCH IMPULSE-TYPE SUPERSONIC

COMPRESSOR ROTOR WITH TURNING

PAST AXIAL DIRECTION

By John J. Jacklitch, Jr., and Melvin J. Hartmann

Lewis Flight Propulsion Laboratory
Cleveland, Ohio

NATIONAL ADVISORY COMMITTEE
FOR AERONAUTICS

WASHINGTON
July 6, 1953

319,98/13

NATIONAL ADVISORY COMMITTEE FOR AERONAUTICS

RESEARCH MEMORANDUM

INVESTIGATION OF 16-INCH IMPULSE-TYPE SUPERSONIC COMPRESSOR

WITH ROTOR TURNING PAST AXIAL DIRECTION

By John J. Jacklitch, Jr., and Melvin J. Hartmann

SUMMARY

A 16-inch impulse-type supersonic-compressor rotor experimentally investigated as a separate component obtained a maximum total-pressure ratio of 5.42 and an adiabatic efficiency of 0.76 at 101-percent design speed. The rotor could be operated over a wide range of back pressures; however, it did not obtain the design impulse condition. At partly closed throttle points, the rotor was able to effect a reduction in equivalent weight flow and total-pressure ratio. This decrease in total-pressure ratio with increased back pressure is a characteristic of a rotor with turning past the axial direction.

The rotor did not operate at either its maximum total-pressure ratio or adiabatic efficiency, or both, for any rotational speed when the diffusing stators were installed. The stators limited the weight flow to very low values at the lower rotational speeds. The stage total-pressure ratio was 3.3, and the stage adiabatic efficiency was 0.51 when the discharge Mach number was reduced to about 0.61 at 101-percent design speed.

A set of flat-plate, constant-area stators installed between the rotor and diffusing stators made the rotor operate nearer its highest performance point. However, the losses in the stators increased with the higher stator-entrance Mach numbers, and the stage performance was not improved.

Peak total-pressure recovery of the stators decreased rapidly as the entering Mach number was increased. The high loading at the rotor discharge may result in a considerable separated region on the rotor, and this poor entrance condition probably contributed to the poor performance of the diffusing stators.

INTRODUCTION

Analytical investigation of the vector diagrams of supersonic compressors (ref. 1) has illustrated the high theoretical total-pressure ratio of the impulse-type supersonic compressor. This compressor rotor

has approximately the same relative entrance and exit Mach numbers at
the mean radius. The problems of design and operation in the low-
pressure-ratio range (rotor turning to less than axial) are discussed
in reference 2, which reports an impulse-type compressor rotor operated
with a total-pressure ratio of 3.6 and an adiabatic efficiency of 0.80.
Increasing the turning in the rotor passage so that the relative flow
direction is axial or beyond results in higher theoretical total-pressure
ratios (ref. 1).

The rotor incorporating turning to less than axial exhibits a con-
ventional performance characteristic, having an increasing work input
with increasing back pressure. However, for the case of rotor discharg-
ing past axial, the work input will decrease with increasing back pres-
sure. The unusual requirement of reducing back pressure to increase the
pressure ratio then results, and the question arises as to the opera-
tional characteristics and stability of a rotor of this type. To inves-
tigate the characteristics of a rotor discharging past axial, the rotor
disk of reference 2 was rebladed. The hub and tip contours were main-
tained and resulted in a discharge angle of about 10° turn past axial to
obtain nearly equal flow areas at entrance and exit to the rotor.

Tests were also carried out to determine the effect of downstream
stators on the operational characteristics of this compressor type as a
complete stage. The performance obtained for the rotor component and
stage investigations is not considered good but is presented to illus-
trate the problems to be encountered with the impulse-type supersonic
compressor.

SYMBOLS

The following symbols are used in this report:

M   absolute Mach number, ratio of absolute fluid velocity to local
        velocity of sound

M'   relative Mach number, ratio of fluid velocity relative to rotor
        to local velocity of sound

N   ratio of compressor speed at point to average compressor speed
        of points at given speed range

P   total or stagnation absolute pressure, lb/sq ft

p   static or stream pressure, lb/sq ft

r   radius, ft

T	total or stagnation temperature, $^\circ$R
U	velocity of rotor, ft/sec
W	weight flow, lb/sec
z	distance along axis of machine, in.
β	angle between compressor axis and absolute fluid direction, deg
δ	ratio of actual inlet total pressure to standard sea-level pressure, $P_1/2116$
η_{ad}	adiabatic efficiency
θ	ratio of actual inlet stagnation temperature to standard sea-level temperature, $T_1/518.6$

Subscripts:

m	mean radius
t	tip
u	compressor rotor component
z	component in axial direction
θ	component in tangential direction
1	entrance-tank instrument station
2	instrument station between rotor and stator
3	instrument station about 8 in. behind rotor or behind stators

APPARATUS

The variable-component test rig used in this investigation was the same as that described in references 2 and 3 and is shown schematically in figure 1. Freon-12 (dichlorodifluoromethane) was used as the test medium.

Rotor Design

The rotor was designed to use as many components of the original compressor as practical. With axial entrance flow (no guide vanes) the hub

and tip contours of the previous design (ref. 2) required 10° turning past the axial direction in the rotor passage to maintain the relative rotor entrance and discharge areas approximately equal. This requirement resulted in a mean-radius rotor-passage turning of 72° and an absolute discharge Mach number of 2.11 for which the vector diagram is shown in figure 2. The number of compressor rotor blades, the blade base, and the attachment were all retained from the previous design so that the original rotor could be rebladed.

The aerodynamic design was limited by the mechanical design of the previous compressor. The hub and tip contours were such that the mean radius remained essentially constant. A mean blade camber line was laid out along this mean radius to obtain the desired turning with a minimum amount of the blade overhanging the base. A suitable thickness distribution was applied to this blade camber line. The blade-surface pressure distribution was determined at the mean radius by considering continuity and the condition of absolute irrotational flow without losses in a manner similar to that of reference 4. The camber line was adjusted to improve the blade-surface pressure distribution until mechanical limitations imposed by the previous design prevented further adjustment. The adjusted mean-radius blade-surface pressure distribution indicates that the latter part of the blade is rather heavily loaded, as shown in figure 3. This blade-surface pressure distribution is not desirable; however, attempts to incorporate increased turning (or loading) at the forward section resulted in a prohibitive overhang of the blade trailing edge. Radial elements were used to determine the blade camber line at all other radii. The blade contours were obtained at three radii by applying the same thickness distribution as used for the mean radius to these blade camber lines. The hub and tip contours and the blade shapes for this 16-inch impulse-type supersonic-compressor rotor are shown in figure 4. A photograph of this compressor rotor is shown in figure 5.

Stator Design

A set of convergent-divergent stators was designed for the open-throttle discharge conditions measured from this supersonic-compressor rotor. These stators were designed for a mean entrance Mach number of about 1.8. The contraction ratio (two-dimensional) was set at 1.14 to allow starting below design speed. A normal shock was considered to exist at the passage throat. The throat was located 37 percent of the mean-radius diffuser-passage width behind the leading edge on the pressure surface and was of constant area for approximately the same length along the blade. The subsonic portion of the blade passage diverged so that on an area basis it was equivalent to a cone with an 8° included angle and was designed to remove all but 10° of the whirl.

2795

The blade was designed at two stations, the hub and the tip, and straight lines were faired between these two sections. Approximate stator-entrance flow angles and Mach numbers were known from the rotor-component investigation. A 12° leading-edge wedge angle was used, and the blade was so oriented that the flow was considered to enter parallel to the suction surface. The passage height was 1.02 inches. A chord length of $5\frac{3}{4}$ inches and the 30 blades result in a mean-radius solidity of 3.70. The blade sections are shown in figure 6 and were installed in the test rig as shown schematically in figure 1.

For a part of this investigation, a set of 30 constant-area stators was installed between the rotor and the diffusing stators to protect the rotor from the static-pressure build-up in the diffusing stator. These stator blades were flat plates of 0.090-inch thickness with the leading and trailing edges sharpened to a 12° wedge. The flat plates were twisted to the approximate measured flow-angle distribution at the rotor discharge and set to give a very slight expansion of the flow for the open-throttle rotor condition.

PROCEDURE

The compressor was tested in Freon-12 with the wheel speed adjusted so that the relative entrance Mach number at the mean radius was the same for air and for Freon-12. The entrance vector diagram at the mean radius for air and Freon-12 is shown in figure 7. The performance of this impulse-type supersonic-compressor rotor as a separate component was determined over a range of back pressures from open throttle to audible surge at seven wheel speeds ranging from 107- to 54-percent design speed. The same computational procedure as described in reference 2 was used. The instrumentation was similar to that of reference 3, with the applicable survey stations renumbered as shown in figure 1.

The over-all performance was obtained by using the measured data at stations 1 and 3. The average total pressure at station 3 was obtained by 15 shielded total-pressure probes arranged to obtain an area-averaged total pressure. The average total temperature was measured by two 3-point double-shielded thermocouple rakes. These instruments are insensitive to wide variations in flow angle, so that the correct readings were obtained by setting the instruments at the average flow angle. The static pressure was measured by static taps on the inner and outer walls. Cone survey instruments were used at stations 2 and 3 to measure total and static pressures and flow angle. The data from these survey instruments could not be obtained at all points (because of mechanical trouble with the probes and the actuators), and the available data were inconsistent. Therefore, the effective average flow angle at station 3 was

calculated from continuity with the measured weight flow and Mach number. (This computation did not allow for a passage boundary layer.)

The diffusing stators were installed about 2.9 inches behind the compressor rotor. The instrumentation was similar to that used in reference 3. Data for the stage operation were obtained in a manner similar to those of the rotor component. The constant-area stators, used for a portion of this investigation, were installed in the space between the rotor and the diffusing stators.

RESULTS AND DISCUSSION

Rotor-Component Investigation

Performance. - The total-pressure ratio measured at the downstream instrument station P_3/P_1 is shown in figure 8. At 101-percent design equivalent speed, a maximum total-pressure ratio of 5.42 was obtained at an equivalent weight flow of 47.3 pounds per second of Freon-12. At this rotational speed, the total-pressure ratio could be reduced to about 4.35 without a change in equivalent weight flow. However, as the total-pressure ratio is reduced from 4.35 to 3.92 by closing the discharge throttle farther, the equivalent weight flow is reduced to about 45.2 pounds per second. The lowest rotor total-pressure ratio is obtained with the throttle closed to the surge point. The variation of total-pressure ratio with back pressure will be discussed in a later section.

The same type of characteristic curve is obtained at 107- and 96-percent design speed. The vertical portion of this characteristic curve was not obtained at the lower equivalent speeds (54, 64, 75, and 85 percent of design). The lower rotational speeds have very little variation in total-pressure ratio, and as the speed is decreased there is an increasing range of equivalent weight flow.

The adiabatic efficiency based on the total-pressure ratio and temperature measurements at the downstream instrument station and in the entrance tank is shown in figure 9. The measured adiabatic efficiency was 0.76 for the peak total-pressure ratio of 5.42 and 101-percent design speed. The adiabatic efficiency fell off rapidly as the throttle was closed, until at the stall point (total-pressure ratio, 3.92) the adiabatic efficiency has been reduced to 0.66. The adiabatic-efficiency curves at all speeds are essentially straight lines that become very nearly vertical (small range of total-pressure ratios) at the lower speeds. A peak adiabatic efficiency of 0.80 at a total-pressure ratio of 2.1 was obtained at 64-percent equivalent speed.

The averaged absolute discharge Mach number behind the rotor and the calculated mean effective discharge flow angle are plotted for the range of total-pressure ratios in figures 10(a) and 10(b), respectively. An absolute discharge Mach number of 1.84 and an average flow angle of about 56° were obtained at 101-percent design speed (open throttle). The discharge Mach number decreases and the calculated discharge angle increases as the total-pressure ratio decreases. The discharge Mach number is about 1.30 and the flow angle is about 62° at the stall point. Similar curves are obtained at all other rotational speeds.

Static-pressure profile along rotor housing. - Static-pressure measurements along the outside housing of the compressor rotor are shown in figure 11 as the ratio of static pressure to entrance total pressure for 101-percent design speed. The key indicates the absolute discharge Mach number and the total-pressure ratio for each operating condition shown. At the open-throttle point $(M_3 = 1.76)$, the ratio of discharge static pressure to inlet static pressure on the outer wall is about 1.38; whereas the design requires the inlet and discharge static pressures at the mean radius to be approximately equal (constant rotor passage area). Throttling results in a general increase in static pressure over the rotor at the outside wall (fig. 4). These static-pressure profiles do not specifically determine the presence, location, or orientation of a shock configuration on the rotor. However, it does appear even at the open-throttle condition that there is some compression in the rear portion of the rotor.

Discussion. - The characteristic curve of this compressor rotor indicates a small range of equivalent weight flows at high speeds. This reduction in weight flow is obtained near the closed-throttle point with high static back pressures (total-pressure ratio of 4.6 and below at 101-percent design speed; see fig. 8). At this condition the relative discharge Mach number is subsonic. The transition from supersonic to subsonic relative Mach number apparently takes place at the entrance to the rotor passage, and thus some reduction in the equivalent weight flow can be obtained before surge occurs.

The characteristic curve of this compressor rotor also indicates that the peak total-pressure ratio was obtained at the open-throttle point. As the throttle was closed (increasing back pressure) the total-pressure ratio was decreased. The reason for this reduction in total-pressure ratio can be shown with the vector diagram in figure 2. The high design total-pressure ratio was obtained with a high discharge whirl component $M_{\theta,2}$ by turning in the rotor passage beyond the axial direction. As the throttle is closed and some diffusion is obtained on the rotor, there is a reduction in M'_2, which, after vector addition, results in a decrease in the discharge whirl component and available total-pressure ratio. This decrease in available total-pressure ratio with

total-pressure ratio and adiabatic efficiency are approximately constant up to a Mach number of about 0.75 and fall off slightly at higher discharge Mach numbers. The performance of the compressor stage is lower than expected, and some of the problems encountered will be considered in the following sections.

Effect of stators on rotor operation. - The stators seem to impose a back pressure on the rotor and thus prevent it from operating at the best performance point (open-throttle condition) determined for the rotor-component investigation. The operating condition of the rotor can be obtained for a part of the performance map by matching the equivalent weight flow for the stage (fig. 12(a)) to the corresponding weight flow for the rotor-component investigation (fig. 8). The stage operates at weight flows near the lower (surge) limit for the rotor as a separate component for 54- and 64-percent design speed. For 75- and 85-percent design speed the measured weight flow for the stage is even lower than the lower limit for the rotor as a separate component. The stage seems to be operating somewhat above the surge weight flow of the rotor at 96-percent design speed. At the higher speeds the equivalent weight flow seems to be just about equal to the maximum weight flow for the rotor as a separate component. (Note that these two figures cannot be compared directly at the highest speed because of the slight difference in speed.) Because of the vertical characteristic of the rotor in this region, the operating point of the rotor is not well defined by the equivalent-weight-flow measurement.

In the region where the measurement of equivalent weight flow does not completely define the rotor operational point, the measured input equivalent power $(hp/\sqrt{\theta\delta}\ N^3)$ based on the measured electric power to the drive motor of the stage was used as a means of comparing stage data with rotor data. In figure 13 the total-pressure ratio, the adiabatic efficiency, and the discharge Mach number for the rotor as a separate component and for the rotor and stator stage at 107-percent design speed are indicated over the range of equivalent horsepower. The equivalent horsepower for the rotor component could be varied from about 1500 to 1740. However, for the stage investigation with the single row of diffusing stators, all the data points are between 1600 and 1680 horsepower.

For this stage investigation, the open-throttle point resulted in expansion to very high Mach numbers through the stators (107-percent design speed). Increasing the back pressure reduced the measured discharge Mach number to about 0.75 without affecting the operational point of the rotor as noted from the equivalent powers. Decreasing the discharge Mach number below 0.75 results in rotor movement to lower equivalent powers and in increasing stage total-pressure ratio and adiabatic efficiency. These data indicate that in the stage investigation the rotor was not operating at maximum total-pressure ratio and adiabatic

efficiency (fig. 13). Curves drawn from 101- and 96-percent design speed (not included) indicate similar regions of operation; however, the rotor is further from its best operating condition. The high total-pressure ratios and adiabatic efficiencies of the rotor obtained when the rotor was operated at open-throttle condition could not be reached in the stage investigation. Surge occurred at a higher weight flow for the stage than for the compressor rotor as a separate component at 107-percent design speed. This fact is apparently a result of the operating characteristics of the stators. The stators very severely limit the weight flow at the lower rotational speeds and thus force the rotor to operate at low levels of adiabatic efficiency.

The diffusing stators would not allow the rotor to operate at its peak performance point. In order to protect the rotor from the back pressure or disturbances caused by the stators, a small set of constant-area stators (described in a previous section) was installed at a slight positive angle of attack between the rotor and the diffusing stators. The performance for the stage with the constant-area stators is shown for 107-percent design speed in figure 13. The range of equivalent horsepowers is 1680 to 1730 as compared with 1600 to 1680 for the diffusing stators alone. Thus it appears that the rotor can now be operated somewhat closer to its peak total-pressure ratio and adiabatic-efficiency point. The stage performance for this configuration, however, is slightly lower than for the diffusing stators alone. The increased Mach number entering the stators apparently increases the diffusion losses to such an extent that they offset any gain from the increased rotor performance.

Stator performance. - For stator discharge Mach numbers below 0.75, the rotor operated over a range of conditions as indicated in figure 13. As the stator discharge Mach number is reduced, the rotor discharge Mach number, adiabatic efficiency, and pressure ratio also reduce. However, the slight increase in stage pressure ratio and efficiency indicates that the improved stator performance at the reduced entrance Mach numbers more than offsets the reduction in rotor performance.

The static-pressure profile over the stators for minimum back pressure (fig. 14, bottom curve) has a stator-entrance Mach number of 1.72 and indicates supersonic flow throughout. Tabulated values of discharge Mach number, stage total-pressure ratio, and adiabatic efficiency are shown to identify the points on figure 13. The middle curve (fig. 14) shows a static-pressure profile similar to that which would be expected with a shock configuration just behind the passage minimum section area as designed. The static-pressure profile for this passage at the maximum back pressure is shown by the top curve of figure 14. The increase in static pressure at instrument station 2 may be caused by pressure disturbances propagated ahead of the stator blade row through the boundary layer; or it may exist because the value plotted is the average of four different taps, some of which may be located near stator passages that may be operating at higher static-pressure levels.

2795

CZ-2 back

The peak total-pressure recovery across the stators for each rotational speed and corresponding Mach number entering the stators is given in figure 15 for both stator configurations. These data were obtained by locating the operational point of the compressor rotor by the methods described in the previous section. Then the downstream measurements for the rotor as a separate component were combined with the discharge conditions of the stage investigations. It is noted that the peak total-pressure recovery falls off very rapidly with increasing entrance Mach number. The peak total-pressure recovery for the diffusing stators at 107-percent design speed was 0.73 and occurred at the minimum entrance Mach number of 1.48. With the constant-area stators installed between the rotor and the diffusing stators, the entrance Mach number to both sets of stators was about 1.8 with the total-pressure recovery of about 0.57 over both stator rows. All the data points shown on this figure are the peak recoveries obtained for a particular rotational speed and result in discharge Mach numbers of less than 0.61.

The recovery for the stators of this investigation is appreciably below that obtained with usual convergent-divergent supersonic diffusers. However, the entrance conditions for the stators will generally include appreciable hub and tip boundary layers as well as mixing losses due to blade wakes, so that efficient diffusion becomes quite difficult. Also, for this investigation, the compressor rotor, through design compromise, may have a considerable separated region at its trailing edge. It is likely that this separation results in unsteady conditions entering the stators and contributes to their poor performance.

SUMMARY OF RESULTS

The results obtained from the investigation of the 16-inch impulse-type supersonic compressor with rotor turning past the axial direction as a separate component and as a stage are summarized below:

1. The rotor could not be operated at the design impulse condition. However, it could be operated continuously over a wide range of back pressures from open throttle to surge.

2. The rotor produced a maximum total-pressure ratio of 5.42 and an adiabatic efficiency of 0.76 at 101-percent design speed and minimum back pressure obtainable. The high rotor turning resulted in a discharge Mach number of 1.84 and a mean calculated flow angle of 56°. A small range of equivalent weight flows exists even at design speed.

3. The theoretical and experimental total-pressure ratio decreases with increased diffusion relative to the rotor passage as a result of the turning past the axial direction.

4. The rotor did not operate at its maximum total-pressure ratio and adiabatic efficiency for any rotational speed when the diffusing stators were installed. Very low equivalent stage weight flow was obtained at low rotational speeds.

5. Small constant-area stators could be used to make the rotor operate closer to its best performance point. However, the total loss over both sets of stators appeared to increase with Mach number, so that the stage performance did not improve.

6. The measured stage (rotor and diffusing stators) total-pressure ratio was 3.3, and the stage adiabatic efficiency was 0.51 at a discharge Mach number of 0.61 at 101-percent design speed.

7. The best stage performance was not obtained at the design point of stators but at the minimum stator-entrance Mach number.

8. Peak total-pressure recovery over the stators decreases rapidly with increased entrance Mach numbers.

9. The losses attributed to the stators may be partly due to the mixing losses caused by rotor blade separation arising from the undesirable rotor blade-loading distribution.

Lewis Flight Propulsion Laboratory
    National Advisory Committee for Aeronautics
        Cleveland, Ohio

REFERENCES

1. Wright, Linwood C., and Klapproth, John F.: Performance of Super-
    sonic Axial-Flow Compressors Based on One-Dimensional Analysis.
    NACA RM E8L10, 1949.

2. Ullman, Guy N., Hartmann, Melvin J., and Tysl, Edward R.: Experi-
    mental Investigation of a 16-Inch Impulse-Type Supersonic-Compressor
    Rotor. NACA RM E51G19, 1951.

3. Klapproth, John F., Ullman, Guy N., and Tysl, Edward R.: Performance
    of an Impulse-Type Supersonic Compressor with Stators. NACA RM
    E52B22, 1952.

4. Stanitz, John D., and Prian, Vasily D.: A Rapid Approximate Method
    for Determining Velocity Distribution on Impeller Blades of Cen-
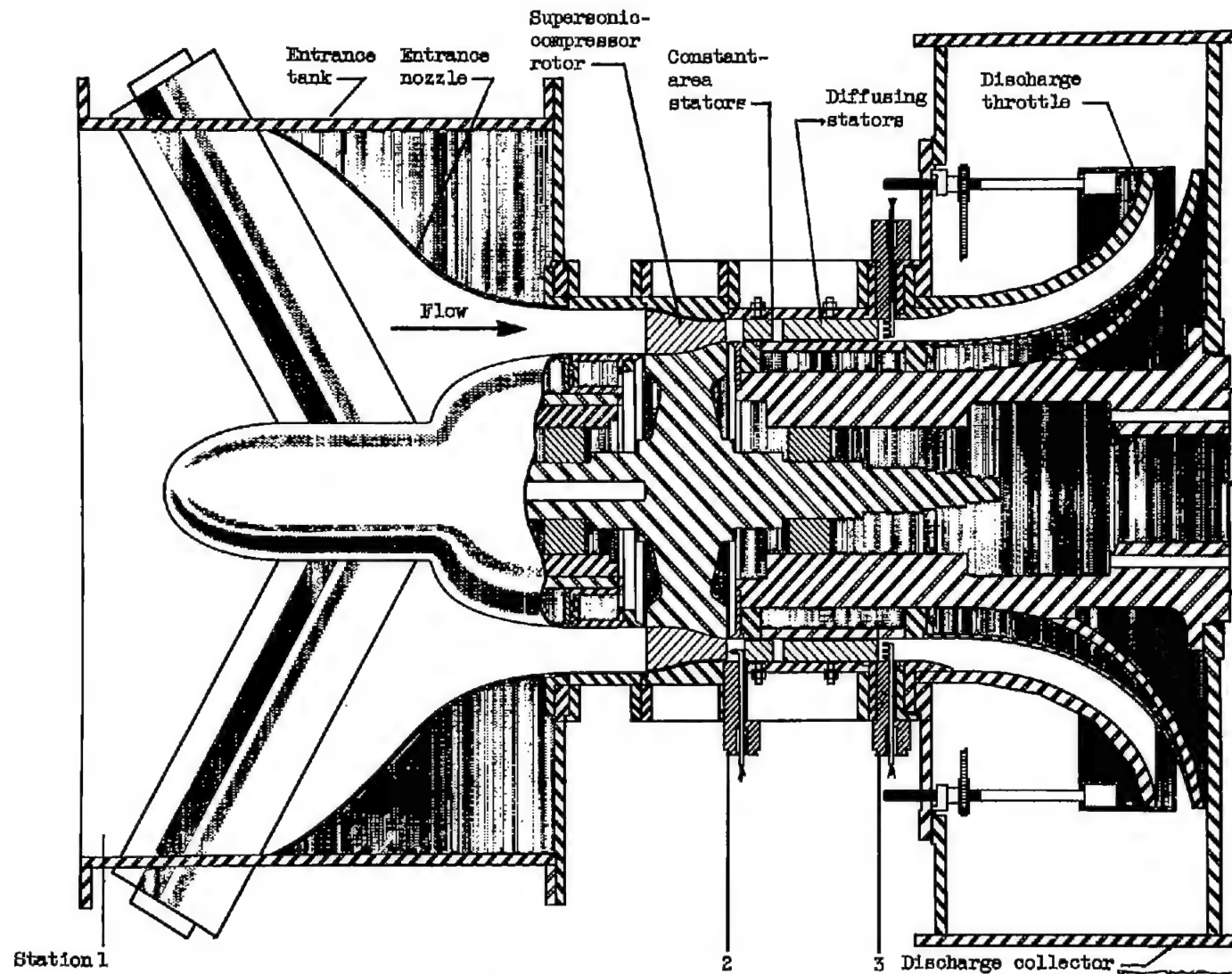   trifugal Compressors. NACA TN 2421, 1951.

Figure 1. - Schematic diagram of variable-component supersonic-compressor test rig.
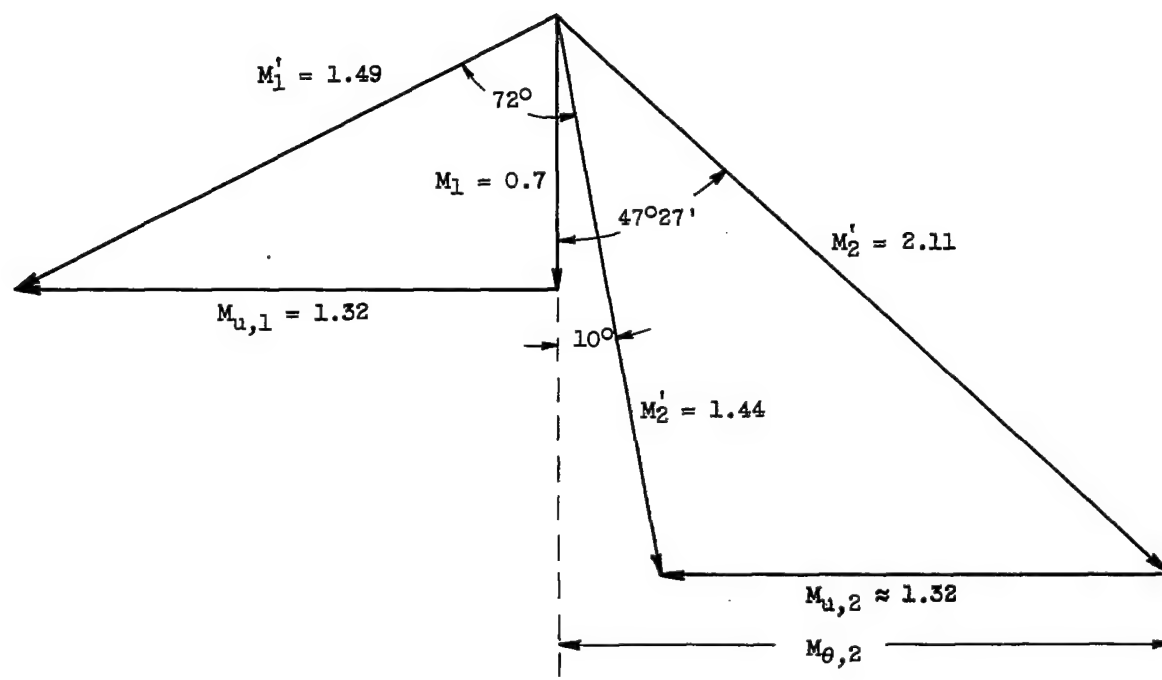
CD-3012

Figure 2. - Design vector diagram for mean radius of 16-inch impulse-type supersonic-compressor rotor with turning past axial direction.
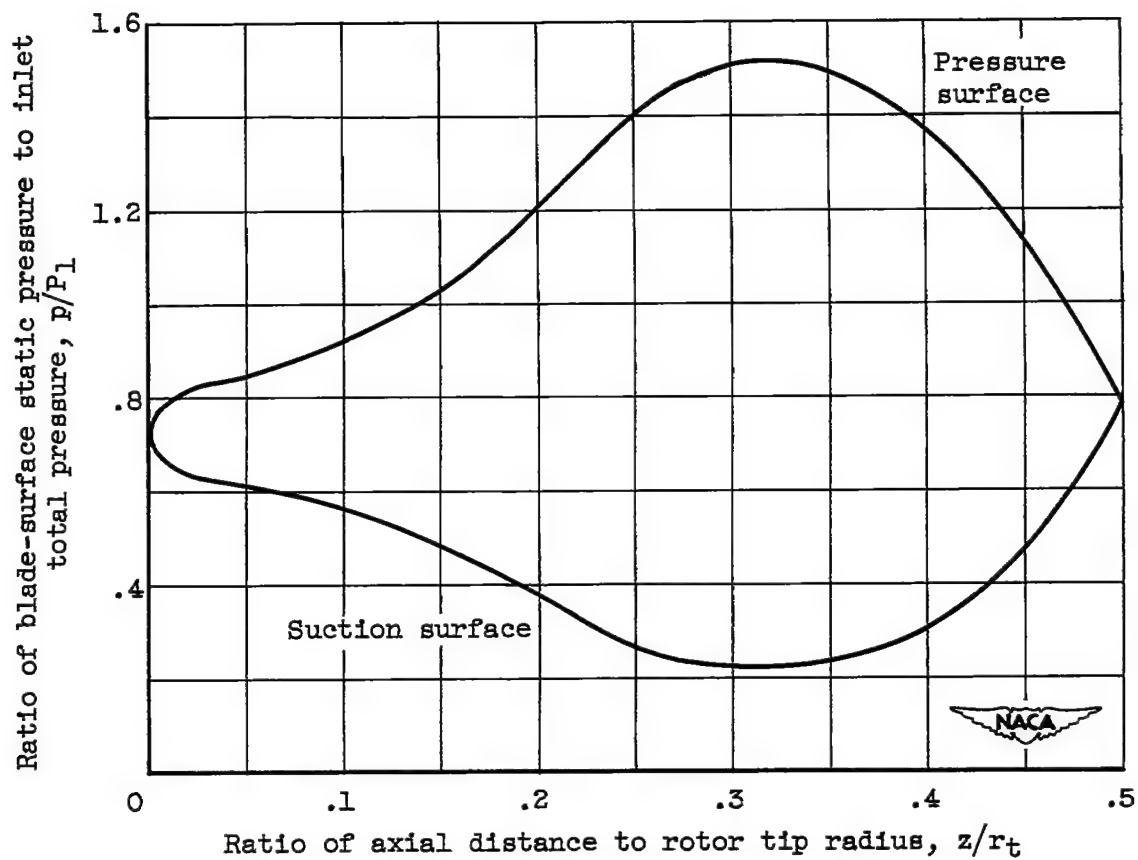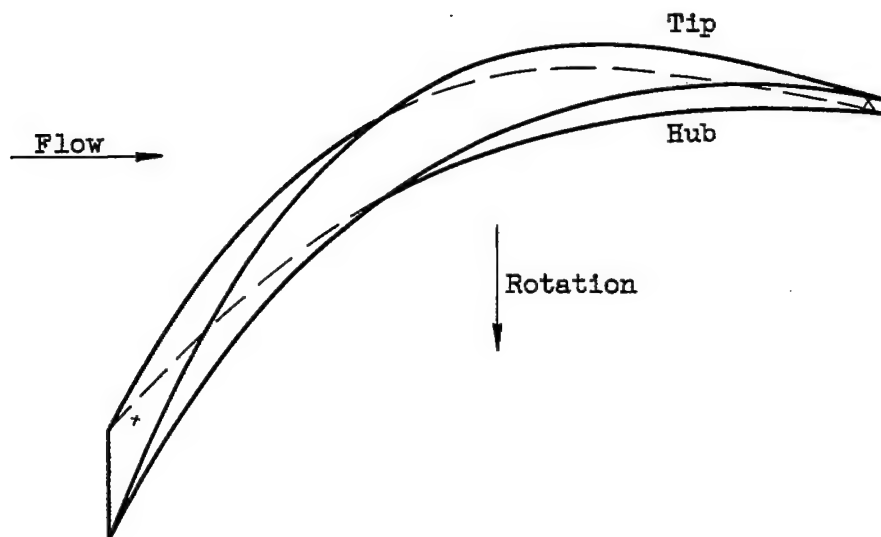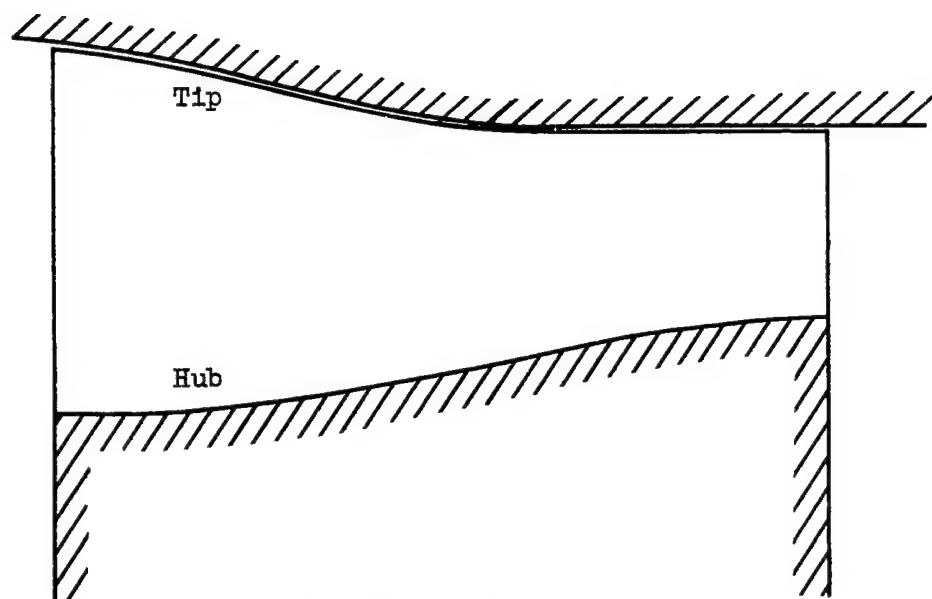
Figure 3. - Blade pressure distribution at mean radius for
impulse-type supersonic-compressor rotor with turning 10°
past axial direction.

2795

(a) Blade shape.

(b) Blade contour.

Figure 4. - Sixteen-inch impulse-type supersonic-
compressor blade with turning past axial direction.

2795

CZ-3
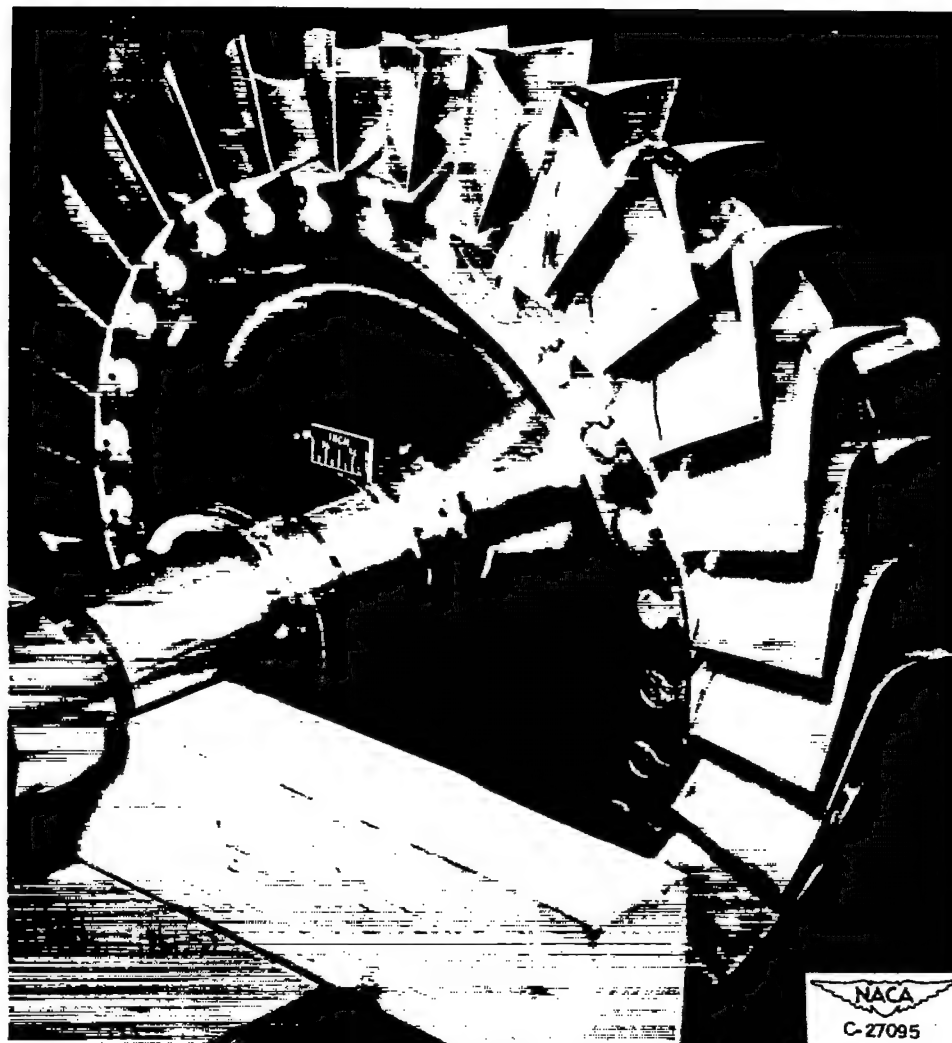
Figure 5. - Sixteen-inch supersonic-compressor rotor (rebladed compressor rotor).
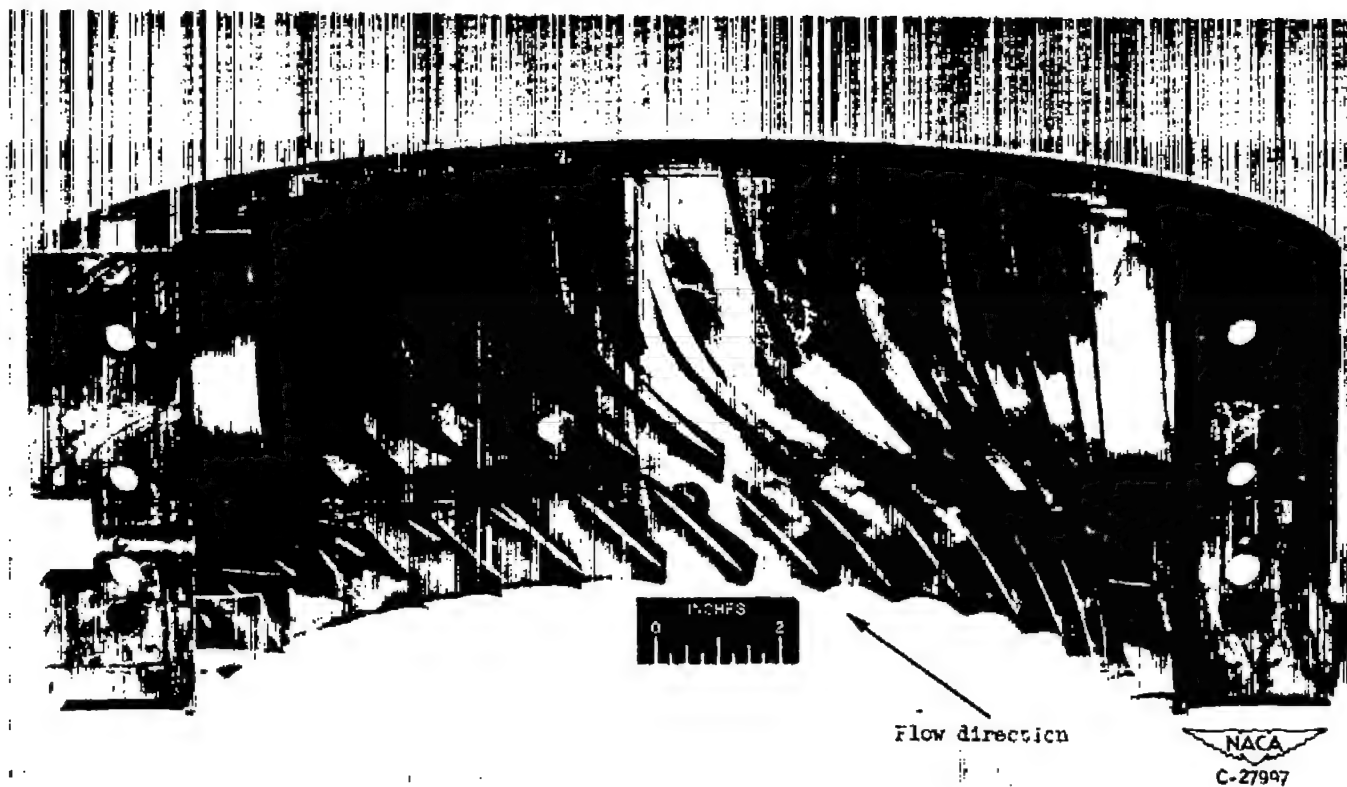
Figure 6. - Stators used with 16-inch impulse-type supersonic-compressor rotor passage turning past axial direction.

2795

CZ-3 back

(a) Design for air.

$M'_m = 1.49$ $M_m = 0.7$

$M_m = 1.32$ $U_m = 1407$ ft/sec

(b) Computed for Freon-12.

$M'_m = 1.49$ $M_m = 0.7$

$M_m = 1.32$ $U_m = 633$ ft/sec
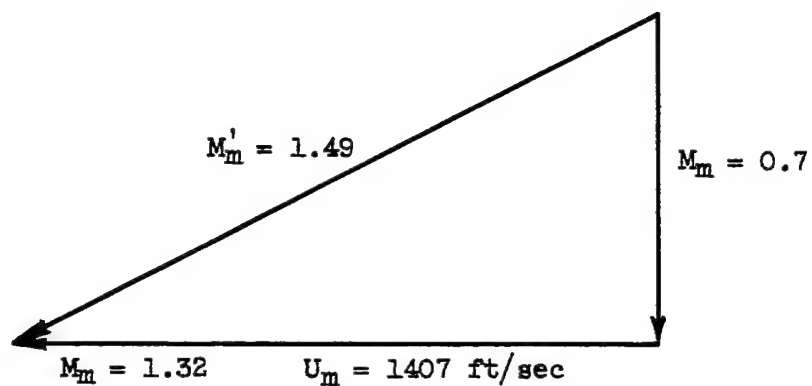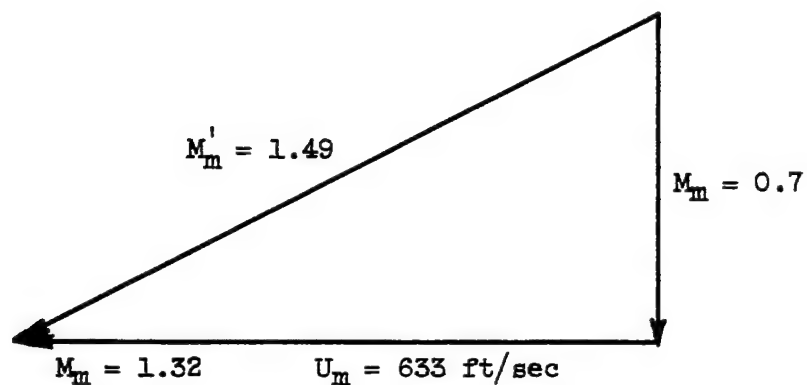
Figure 7. - Design entrance diagram for air and
    Freon-12 at mean blade radius for 16-inch
    impulse-type supersonic-compressor rotor with
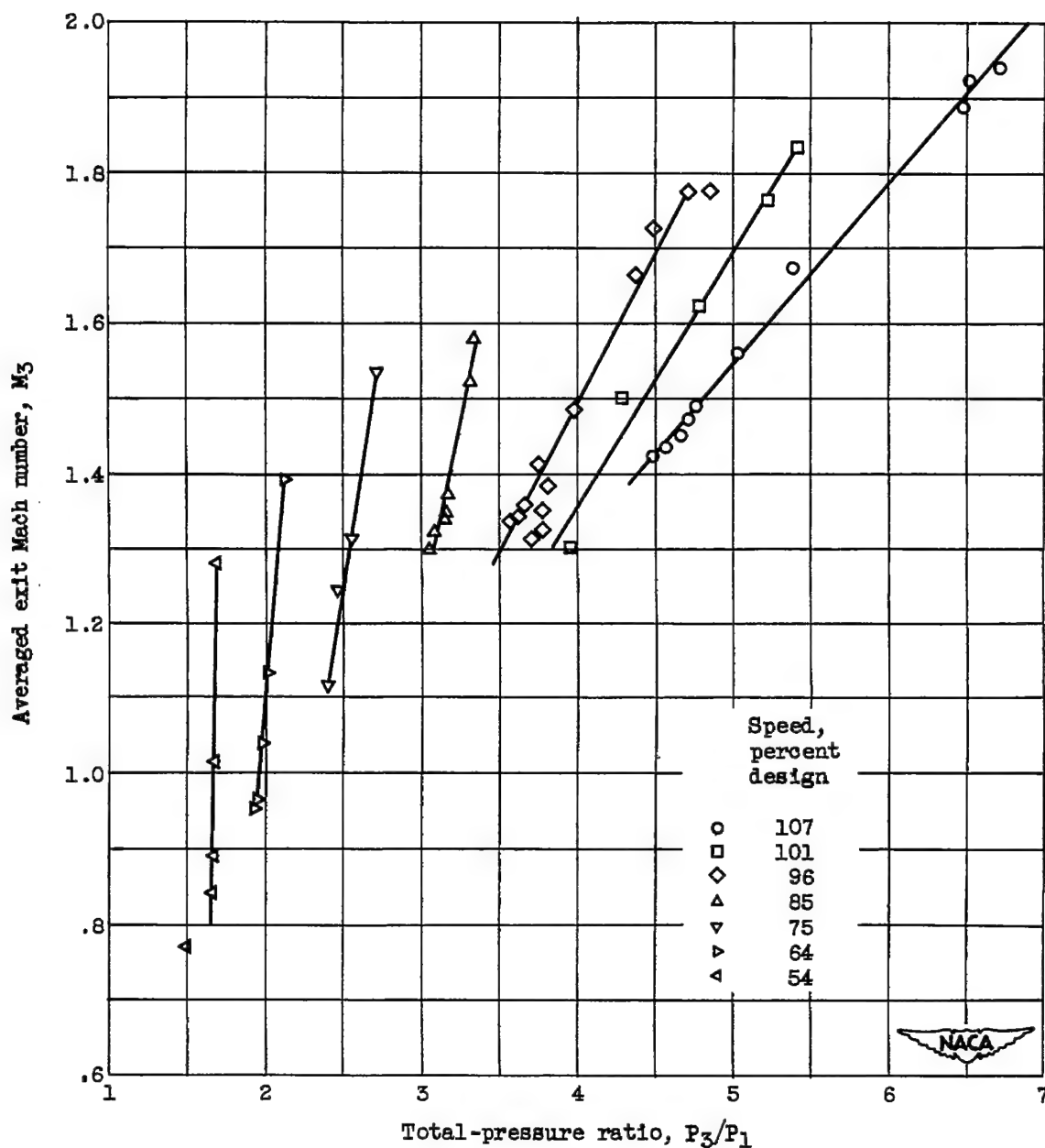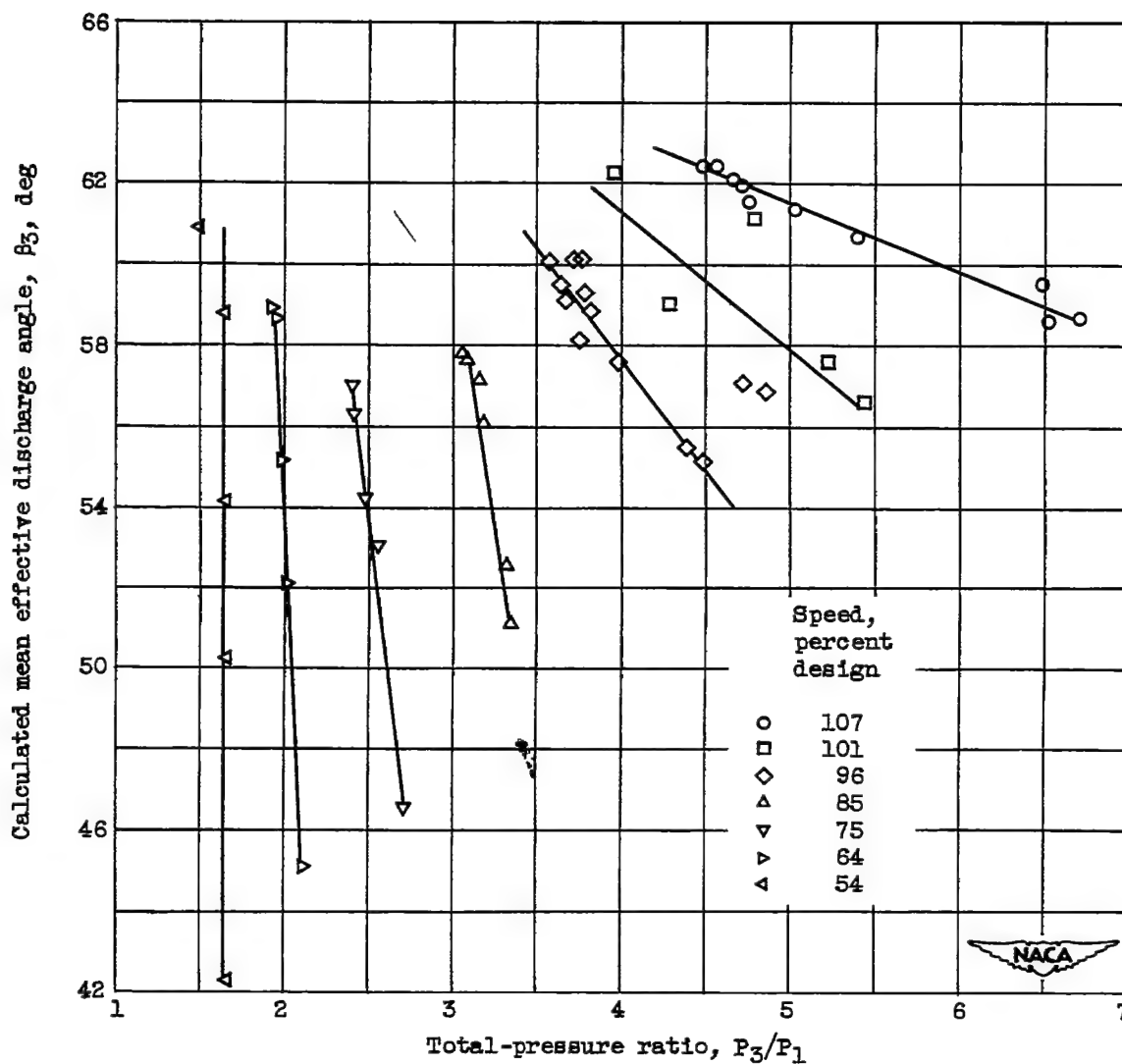   turning past axial direction.
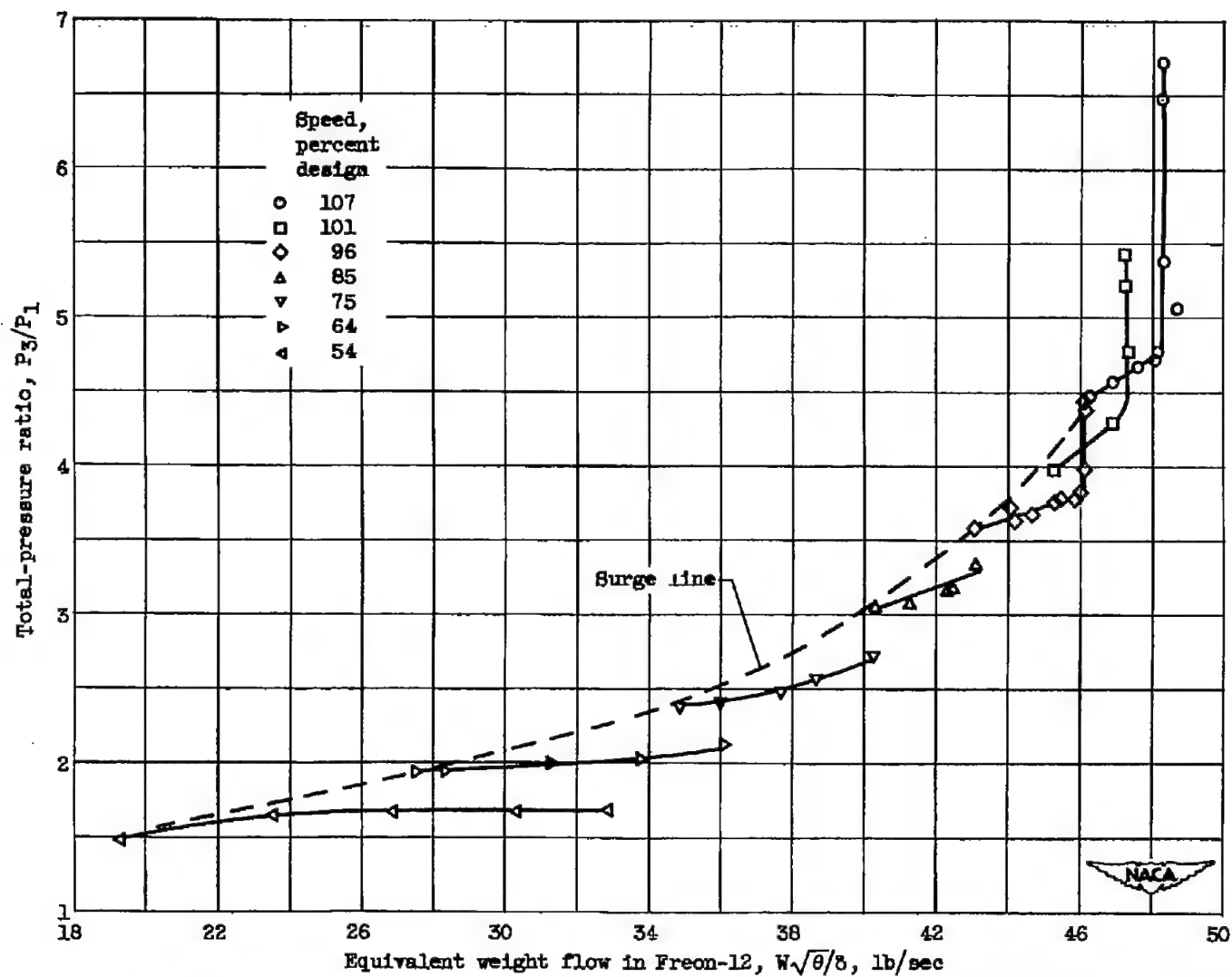
Figure 8. – Performance characteristics of 16-inch impulse-type supersonic-compressor rotor with turning past axial direction at seven equivalent speeds.

Figure 9. - Variation of total-pressure ratio with adiabatic efficiency
for 16-inch impulse-type supersonic compressor with turning past axial
direction at seven equivalent speeds.
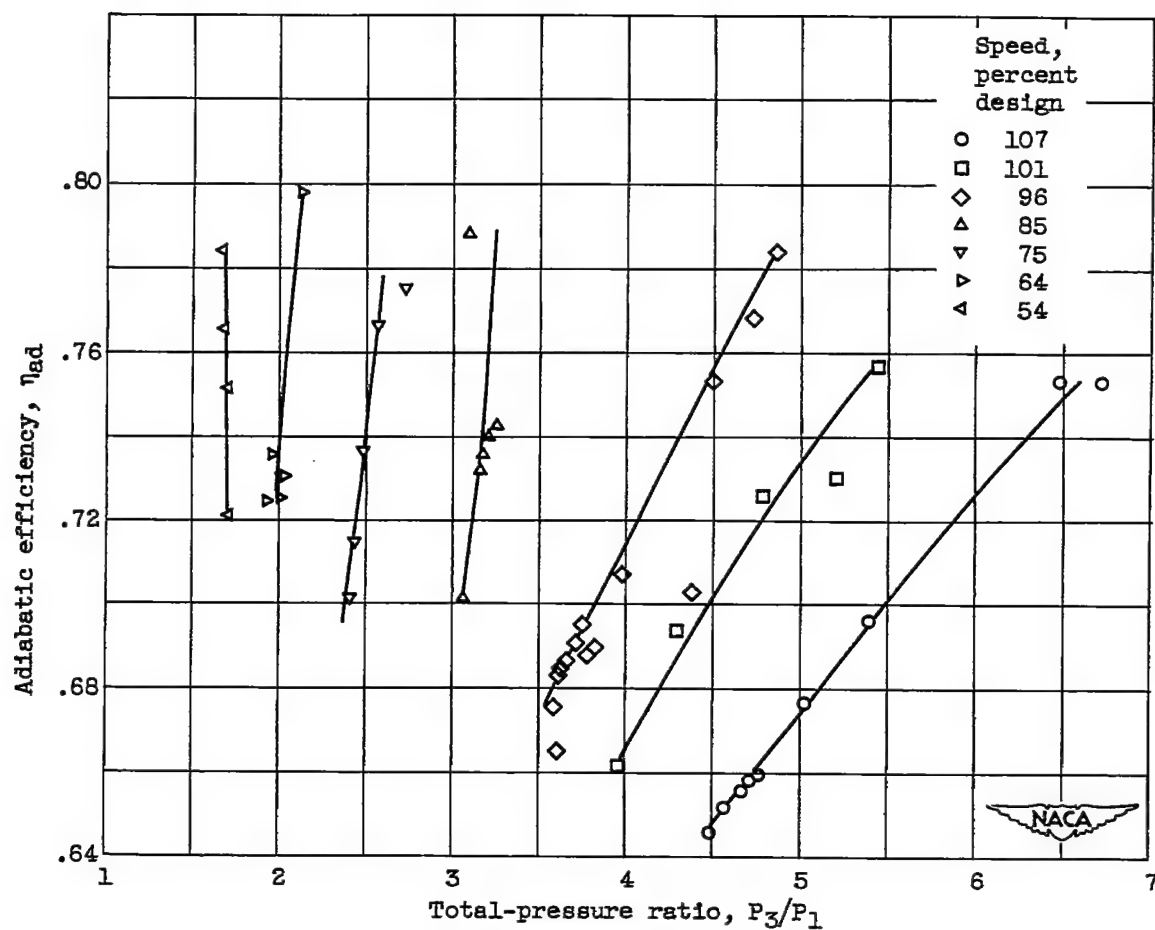
(a) Exit Mach number.

Figure 10. - Variation of exit Mach number and calculated mean discharge angle with total-pressure ratio for 16-inch impulse-type supersonic-compressor rotor with turning past axial direction.
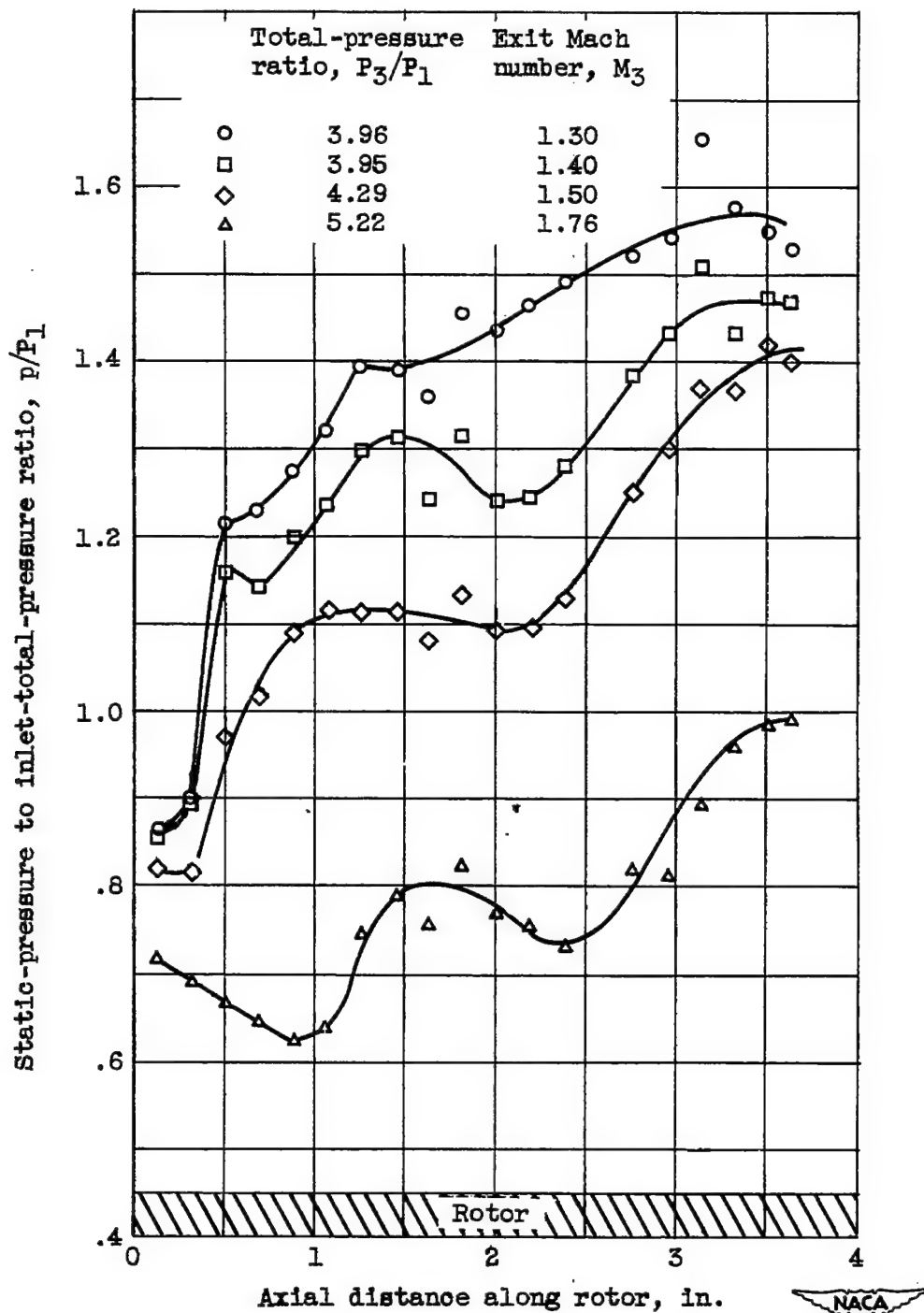
2795

(b) Calculated mean discharge angle.

Figure 10. - Concluded. Variation of exit Mach number and calculated mean
discharge angle with total-pressure ratio for 16-inch impulse-type
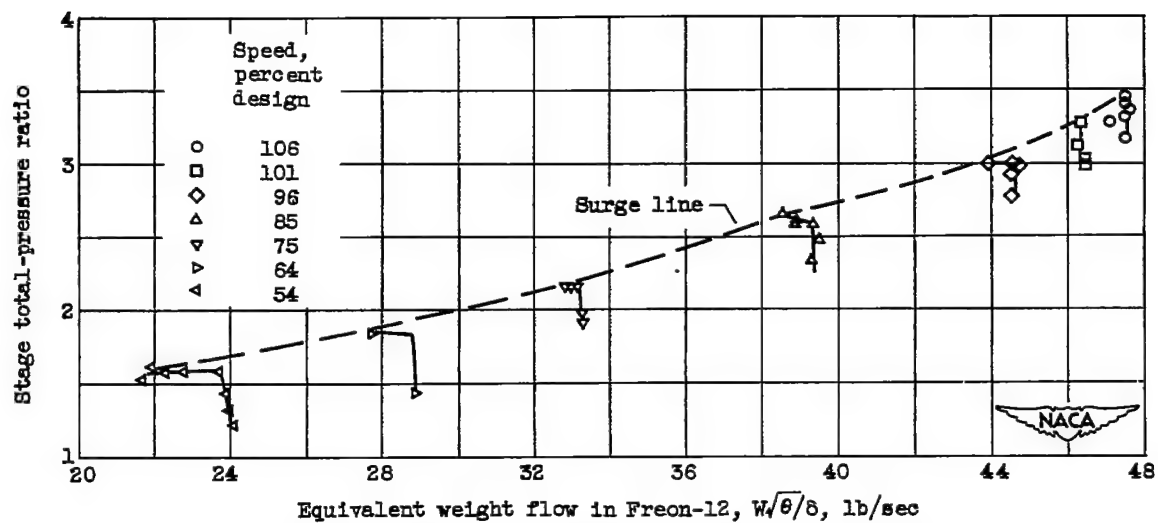supersonic-compressor rotor with turning past axial direction.

Figure 11. - Static-pressure profiles over rotor housing for 16-inch impulse-type supersonic-compressor rotor with turning past axial direction. Speed, 101-percent design.

(a) Total-pressure ratio and weight flow.

Figure 12. - Stage characteristics of 16-inch impulse-type supersonic-compressor rotor with diffusing stators.
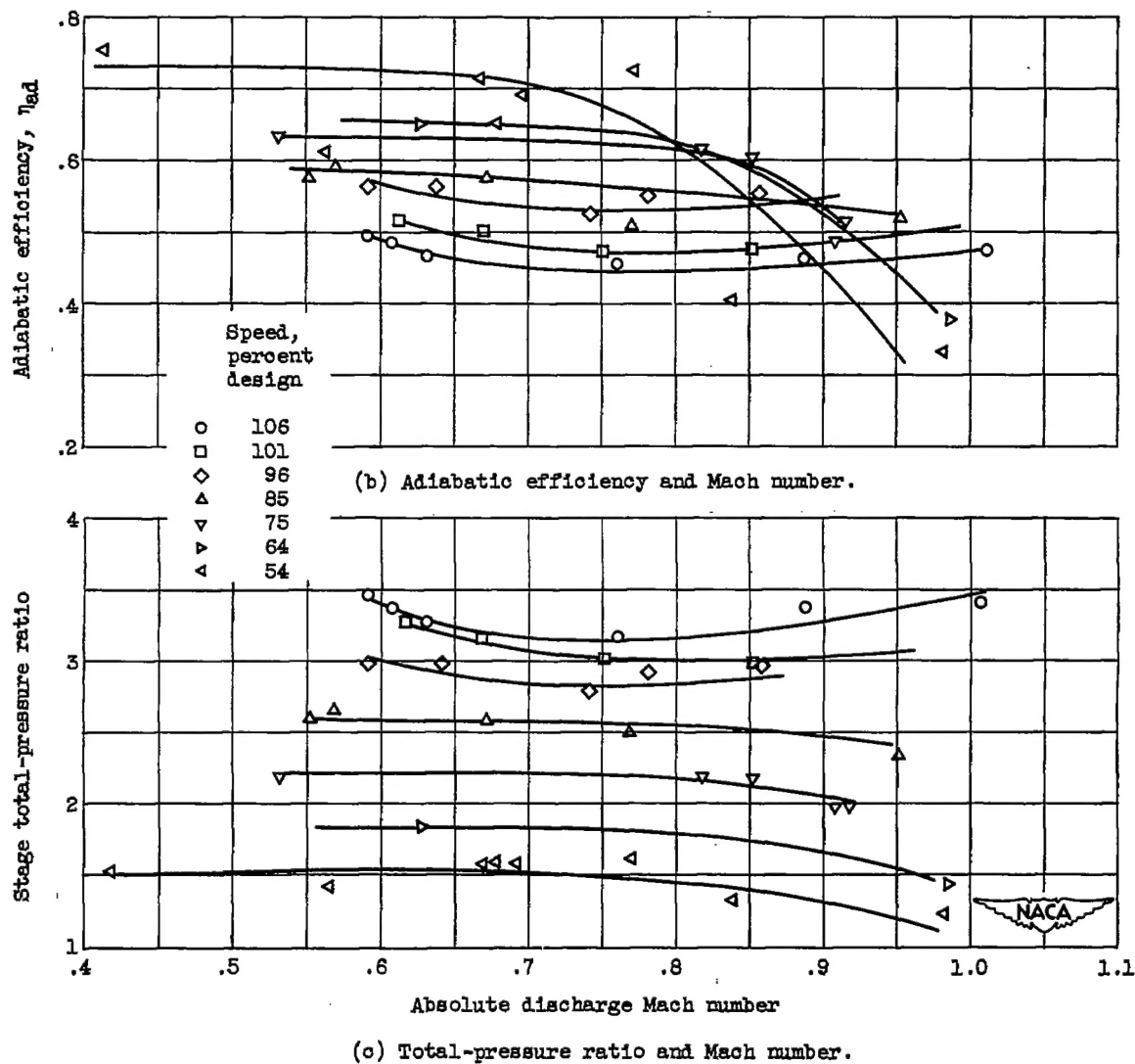
(b) Adiabatic efficiency and Mach number.

Speed, percent design	
○	106
□	101
◇	96
△	85
▽	75
▷	64
◁	54

(c) Total-pressure ratio and Mach number.

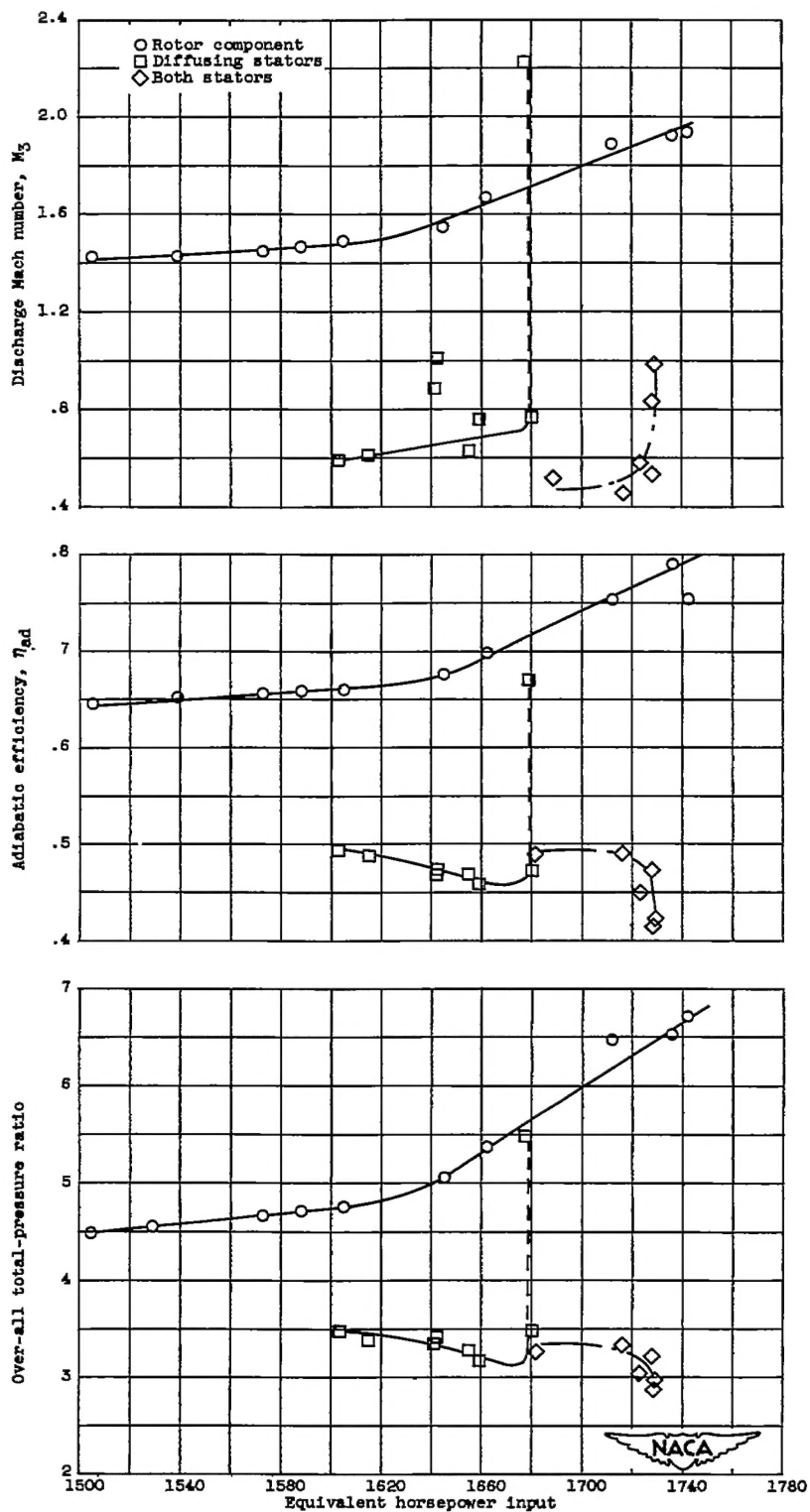Figure 12. - Concluded. Stage characteristics of 16-inch impulse-type supersonic-compressor rotor with diffusing stators.

Figure 13. - Performance of impulse-type supersonic-compressor rotor with
turning past axial direction as a separate component and as a stage with
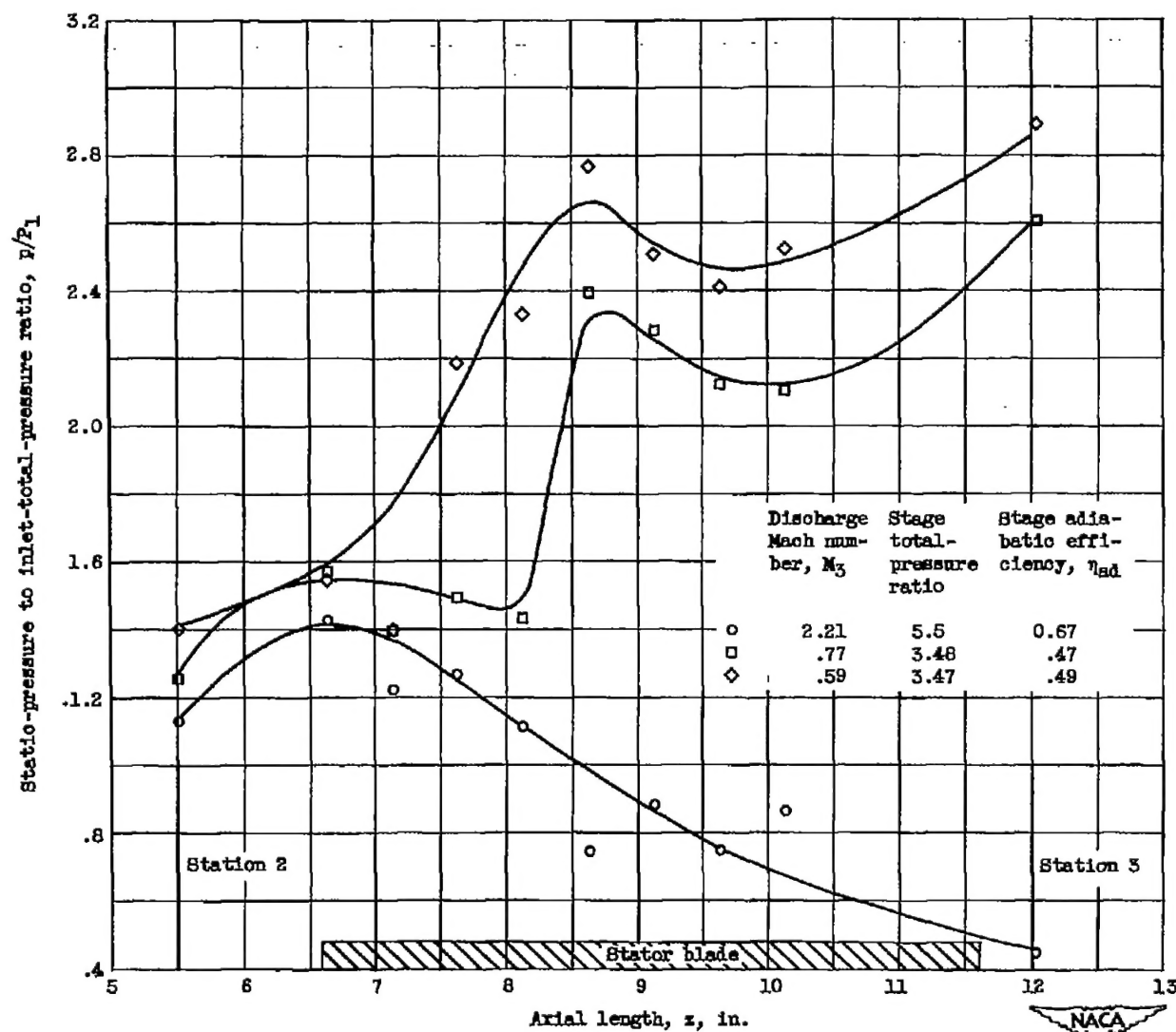diffusing stators. Speed, 107-percent design.

Figure 14. - Static-pressure profiles over stator housing. Diffusing stators used behind 16-inch supersonic-compressor rotor with turning past axial direction. Speed, 107-percent design.
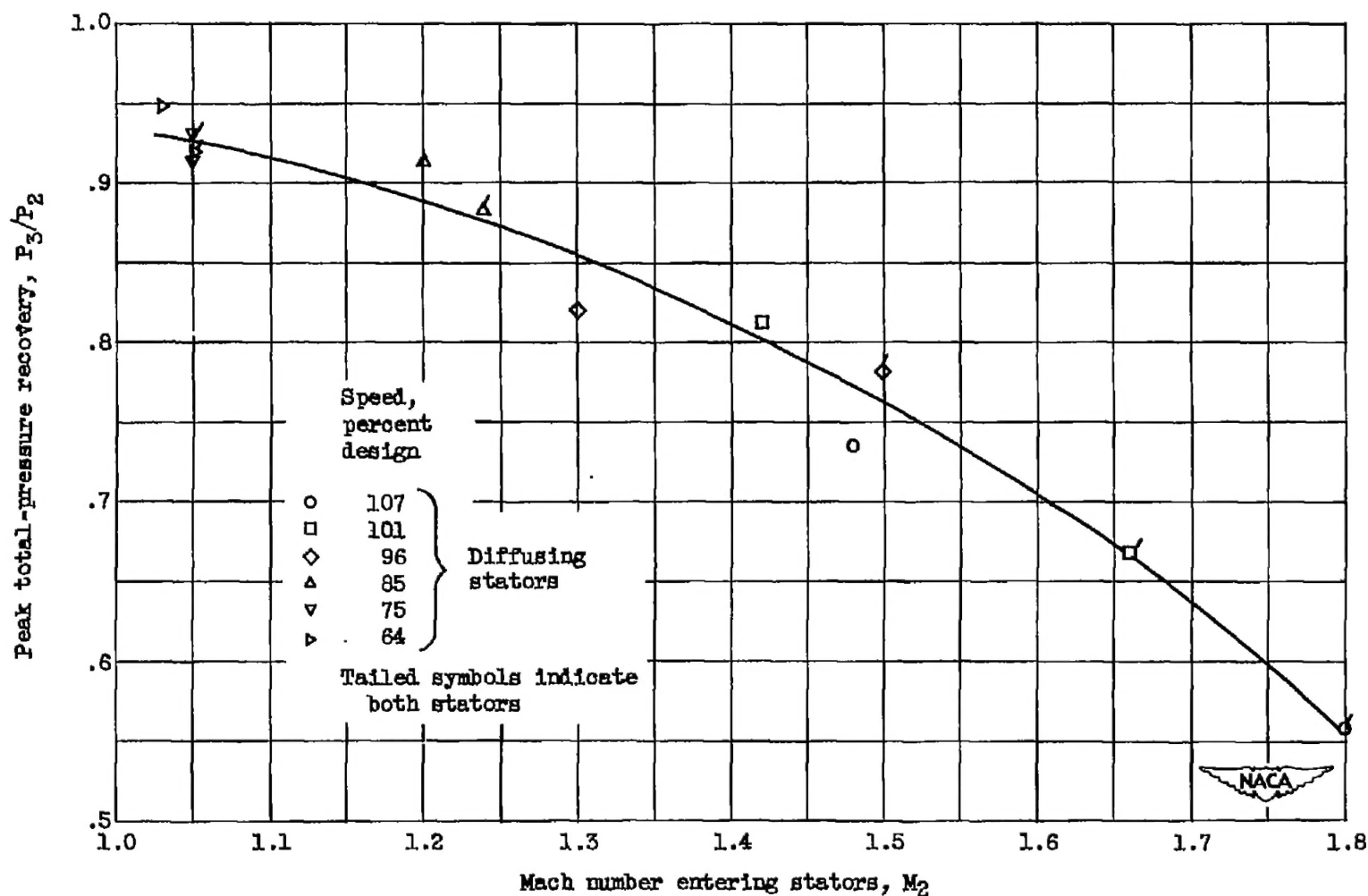
Figure 15. - Peak total-pressure recovery over stators when installed behind 16-inch supersonic-compressor rotor with turning past axial direction.